Emergent Materials (2023) 6:1319–1327
https://doi.org/10.1007/s42247-023-00523-x

ORIGINAL ARTICLE

Exploring the structural, electronic, optical properties and stability of Na_2SrX (Si and Ge) full-Heusler alloys: A first principle investigation

Charef Abbes[1] · Souheil Belbachir[2] · Hamza Abbassa[1] · Said Meskine[1] · Abdelkader Boukortt[1]

Received: 22 March 2023 / Accepted: 9 June 2023 / Published online: 19 June 2023
© Qatar University and Springer Nature Switzerland AG 2023

Abstract

The full-potential linearized augmented plane wave (FP-LAPW) method, based on the density functional theory (DFT) with the generalized gradient approximation (GGA) plus modified Becke-Johnson (mBJ), are used to study the structural, elastic, electronic, and optical properties of Na_2SrX (Si and Ge) full-Heusler alloys. Our calculations indicate that the studied compounds have a nonmagnetic Hg_2CuTi structure. Calculations of electronic band structures and the densities of states showed that Na_2SrSi and Na_2SrGe compounds exhibit semiconductor behaviour at optimized equilibrium lattice constants, with indirect band gaps along the L–X direction of 0.652 eV and 0.629 eV, respectively. The exciton binding energy in the Wannier-Mott model was found to be 8.58 meV for Na_2SrSi and 6.91 meV for Na_2SrGe. We show that these compounds exhibit dynamic and elastic stability. Moreover, the formation energy suggests that these compounds can be synthesized experimentally. Besides, the optical properties (complex dielectric function, refractive index, reflectivity, and optical absorption) were also examined. The results obtained suggest the potential of these full-Heusler alloys for optoelectronic devices in the ultraviolet range.

Keywords Full-Heusler · GGA-mBJ · Semiconductor · Optical properties · Phonon caculation

1 Introduction

New semiconductors with characteristics that might possibly enhance performance and energy efficiency in electronic devices are the subject of continuing research and development. In recent years, there has been a growing interest among researchers to investigate the potential of Heusler alloys as semiconductors for use in electronic and optoelectronic devices. Heusler compounds, named after Fritz Heusler [1], are a family of materials that have gained significant attention due to their diverse properties [2, 3] and potential technological applications [4–16]. They are classified into two categories [3]: half-Heusler (HH) with a general chemical formula of XYZ and full-Heusler (FH) represented by X_2YZ, with quaternary Heusler (QH) with XX'YZ composition closely associated with the full-Heusler alloys. X, X' and Y can be a transition, alkali and alkaline earth metals and Z is a main group element. Most HH compounds with 18 valence electrons per formula unit have a semiconducting behavior [17, 18] and have received great attention as promising semiconductors for various applications such as thermoelectrics, transparent conductors, topological insulators, and buffer layers of solar cells. On the other hand, this behavior is rare in quaternary and full-Heusler alloys. However, a semiconductor character is observed for the SH and QH compounds, which have 24 valence electrons per formula unit [19–26]. Recent studies [27–32] have focused on exploring the structural, electronic, vibrational, and

✉ Charef Abbes
charef.abbes@univ-mosta.dz

Souheil Belbachir
souheil.belbachir@univ-mosta.dz

Hamza Abbassa
hamza.abbassa@univ-mosta.dz

Said Meskine
said.meskine@univ-mosta.dz

Abdelkader Boukortt
abdelkader.boukortt@univ-mosta.dz

1 Laboratory of Elaboration and Characterization Physico-Mechanical and Metallurgical of Materials (ECP3M), Abdelhamid Ibn Badis University, Route Nationale N°11, Kharrouba, 27000 Mostaganem, Algeria

2 Laboratory of Analysis and Application of Radiation (LAAR), University of Sciences and Technology Mohamed Boudiaf, 31000 Oran, Algeria

thermoelectrical properties of various quaternary Heusler compounds containing 18 valence electrons per formula unit using first-principles calculations. These studies have shown the investigated materials are mechanically and dynamically stable semiconductors with band gaps in the range 0.2 to 2.5 eV. In their study, Jiangang He et al. [33] predict new stable full-Heusler compounds with 10 valence electrons showing semiconducting behavior with excellent thermoelectric properties. A new family of full-Heusler compounds without transition metals has appeared recently [2], such as Li_2CaC, Li_2SrC [34] and Li_2MgSi [35], which have been shown to have semiconducting properties with band gaps of 1.127 eV, 0.979 eV and 0.2 eV, respectively.

In the context of the search for new semiconductor materials, investigations related to the structural, electronic, elastic and optical properties of the full-Heusler alloys Na_2SrSi and Na_2SrGe were carried out. As far as we know, there are no experimental or theoretical studies of the compounds Na_2SrSi and Na_2SrGe available in the literature. Therefore, our findings may be useful as a prediction for future research, especially for experimentalists.

2 Crystal structure and computational details

The conventional full-Heusler alloys X_2YZ crystallize in the cubic structure in two prototype structures: Cu_2MnAl and Hg_2CuTi prototypes, as shown in Fig. 1. In the Cu_2MnAl-type (Fm3m, space group no. 225), the X, Y and Z atoms are located at A (0, 0, 0) and B (0.5, 0.5, 0.5) sites, C (0.25, 0.25, 0.25) sites, and D (0.75, 0.75, 0.75) sites, respectively. The Hg_2CuTi-type (216, F43m) is obtained by placing X atoms at A (0, 0, 0) and C (0.25, 0.25, 0.25) sites, and Y atoms at B (0.5, 0.5, 0.5). The calculations of the structural, elastic, electronic, magnetic, and optical properties were performed using DFT [36, 37] based on the FP-LAPW method [38], as implemented in WIEN2K package [39]. The electronic exchange–correlation potential is described with the generalized gradient approximation (GGA) [40]. To obtain better and more accurate electronic and optical properties, we have used the modified Becke-Johnson (mBJ) scheme [41]. The convergence of the basis set was controlled by a cutoff parameter $R_{MT}K_{max} = 9$ where R_{MT} is the smallest of the muffin-tin sphere radii and K_{max} is the largest reciprocal lattice vector. The R_{MT} spheres of 2.00 bohr for Na and Si, and 2.20 bohr for Sr and Ge, were adopted. For the integrations over the Brillouin zone, 2000 k-points with a k-mesh of $12 \times 12 \times 12$ are introduced. The cut-off energy, which defines the separation of valence and core states, was chosen as -6 Ry. The energy and charge convergence values were set to 10^{-4} Ry and 0.001 e, respectively. The optical properties and the total density of states (DOS) were performed using a dense Monkhorst–Pack grid of $27 \times 27 \times 27$ k-points [42].

The phonon spectra are calculated by using density functional perturbation theory (DFPT) [43–47] as implemented in the Quantum ESPRESSO code [48, 49]. The Perdew-Zunger (LDA) exchange–correlation pseudopotentials available in the GBRV (Garrity-Bennett-Rabe-Vanderbilt) database [50] are exploited.

3 Results and Discussion

3.1 Structural properties and phase stability

The first very important step is to obtain information about the structural parameters of Na_2SrX (Si and Ge), particularly the lattice constant (a_0), the compressibility modulus B_0 and its derivative B'. This first procedure predicts the most stable phase of the material. Figure 2 represents the energy-volume change curves for Na_2SrSi and Na_2SrGe in the magnetic (FM) and non-magnetic (NM) states for the two atomic arrangements (Cu_2MnAl and Hg_2CuTi). As a result, the more stable structure of the two compounds

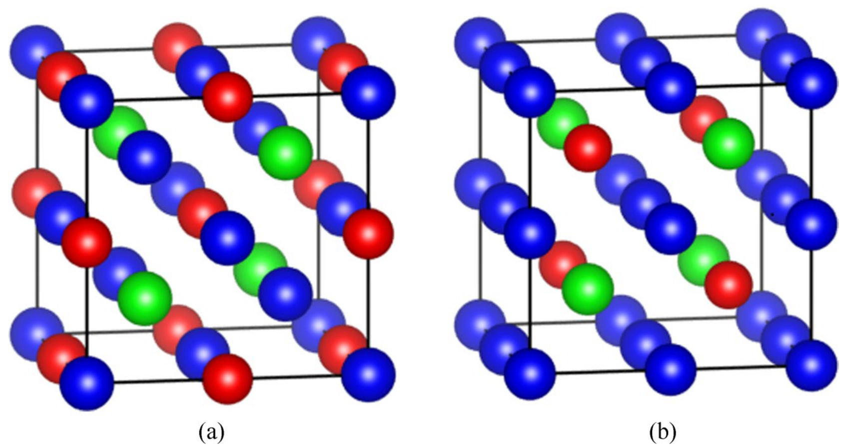

Fig. 1 The crystal structure of the full-Heusler X_2YZ (**a**) Hg_2CuTi-type structure and (**b**) Cu_2MnAl-type structure (blue-Na, Red – Sr, and green-Si/Ge)

Fig. 2 Total energy as a function of volume of Na_2SrSi and Na_2SrGe compounds

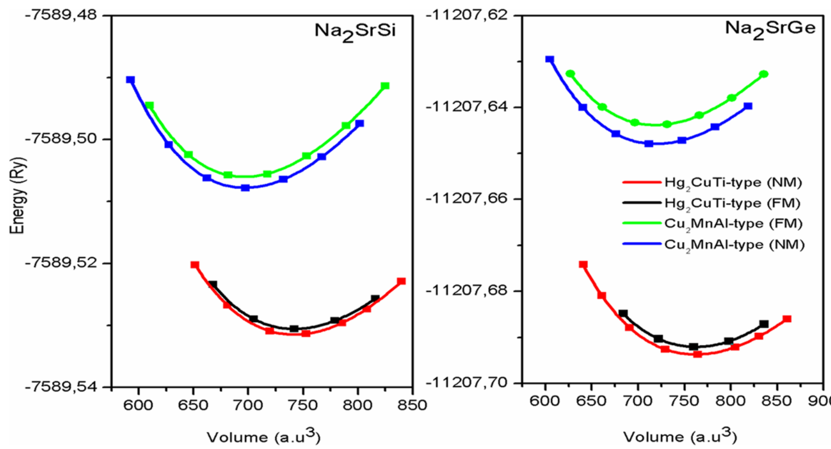

Table 1 Optimized lattice parameters of Na_2SrX (Si and Ge) alloys in the nonmagnetic (NM) state of the Hg_2CuTi structure

Compound	Na_2SrSi	Na_2SrGe
Lattice constant, a_0 (Å)	7.604	7.672
Bulk modulus, B_0 (GPa)	23.925	21.926
Derivative of B_0, B'	4.092	4.157
Total energy, E_0 (eV)/f.u	-7589.531	-11207.693
Formation Energy, E_f (eV)/f.u	-9.703	-9.078
Cohesive Energy, E_{coh} (eV)/f.u	-0.847	-1.178
Band gap E_g (eV)	0.652	0.629
Static dielectric constant $\varepsilon_1(0)$	13.122	14.051
Static refractive index $n(0)$	3.622	3.748

Table 2 The calculated elastic properties of Na_2SrX (Si and Ge) compounds

elastic properties	Na_2SrSi	Na_2SrGe
C_{11} (GPa)	31.13	31.95
C_{12} (GPa)	18.93	17.11
C_{44} (GPa)	25.63	23.58
Bulk modulus, B_0 (GPa)	23	22.06
Shear modulus, G (GPa)	17.82	17.11
Poisson's ratio, ν	0.19	0.19
Young's modulus, E (GPa)	42.48	40.78
Cauchy pressure, C_p (GPa)	-6.70	-6.47
Pugh ratio, B/G	1.29	1.28
Elastic anisotropy factor, A	4.20	3.17

under study corresponds well to the Hg_2CuTi-type structure with a nonmagnetic character. The structural parameters are deduced by fitting the curve of variation of total energy as a function of volume by the Murnaghan equation of state [51]. The results obtained are given in Table 1.

In order to confirm the structural stability and the possibility of synthesizing the Na_2SrX (Si and Ge) alloys experimentally, we calculated the formation (E_f) and cohesive (E_c) energies according to the following formulas [52, 53]:

$$E_f = E_{Total}^{Na_2SrX} - \left(2E_{Na}^{bulk} + E_{Sr}^{bulk} + E_X^{bulk}\right) \quad (1)$$

$$E_c = \left(2E_{Na}^{iso} + E_{Sr}^{iso} + E_X^{iso}\right) - E_{Total}^{Na_2SrX} \quad (2)$$

where $E_{Total}^{Na_2SrX}$ is the equilibrium total energy of the studied compounds under their equilibrium lattice constant, $E_{Na}^{bulk}, E_{Sr}^{bulk}$ and E_X^{bulk} correspond to the total energies per atom of each element in the bulk, $E_{Na}^{iso}, E_{Sr}^{iso} and E_X^{iso}$ are the total energies of the atomic components in the isolated state. The results obtained in Table 1 confirm the thermodynamic stability of these compounds as well as the possibility of their experimental synthesis.

3.2 Mechanical and dynamical stabilities

The elastic properties are deduced from the elastic constants C_{ij} [54]. These coefficients are coupled to the stability and stiffness of the compounds. As both Na_2SrX (Si and Ge) compounds have cubic symmetry, they are characterized by three independent elastic constants, namely: C_{11}, C_{12} and C_{44}, which must meet Born Huang's stability criteria [55] if these alloys are mechanically stable:

$$\begin{cases} C_{11} - C_{12} > 0, C_{11} > 0, C_{44} > 0 \ \ and \\ C_{11} + 2C_{12} > 0 \ \ and \\ C_{12} < B < C_{11} \end{cases} \quad (3)$$

The obtained elastic constants C_{ij} for Na_2SrX (Si and Ge) alloys are presented in Table 2. From the results obtained, we can draw the following conclusions for each of the compounds examined: (i) The mechanical stability in the Hg_2CuTi-type structure with a nonmagnetic (NM) ground state of both Na_2SrSi and Na_2SrGe is confirmed from the positive calculated values of elastic constants (C_{11}, C_{12}, C_{44})

and the required condition for stability. (ii) The value of the bulk modulus derived from the elastic constant is very close to the value computed from the third-order Birch-Murnaghan state equation, indicating the reliability of the theoretical method. (iii) The elastic constants C_{ij} of Na_2SrSi are comparable to those of Na_2SrGe, which implies that these compounds have the same resistance to external stress. (iv) Since $C_{11} > C_{44}$, these compounds display higher resistance to unidirectional deformation compared with shear deformation.

Bulk modulus (B_0), Shear modulus (G), Young's modulus (E), Poisson's ratio (ν), and elastic anisotropy factor (A) are calculated from the calculated C_{ij} values using the Voigt-Reuss-Hill approximation [56–58]:

$$B_0 = \frac{1}{3}\left(C_{11} + 2C_{12}\right) \tag{4}$$

$$G = \frac{1}{2}\left(G_V + G_R\right) \tag{5}$$

$$G_V = \frac{1}{5}\left(C_{11} - C_{12} + 3C_{44}\right) \tag{6}$$

$$G_R = \frac{5C_{44}\left(C_{11} - C_{12}\right)}{4C_{44} + 3\left(C_{11} - C_{12}\right)} \tag{7}$$

$$E = \frac{9BG}{3B + G} \tag{8}$$

$$\upsilon = \frac{3B - 2G}{2(3B + G)} \tag{9}$$

$$A = \frac{2C_{44}}{C_{11} - C_{12}} \tag{10}$$

From the calculated values of the above parameters, we can conclude the following: The Pugh ratio B/G used to predict the brittle (B/G < 1.75) or ductile (B/G > 1.75) character of materials is about 1.29 for Na_2SrSi and 0.96 for Na_2SrGe, so Na_2SrX (Si and Ge) alloys reveal their brittle nature. This behavior is confirmed by the Cauchy pressure ($C_P = C_{12}$- C_{44}) because the brittle character occurs when $C_P < 0$, clearly this is the case in our situation. The Poisson ratio ν is a useful parameter for characterizing the mechanical behavior of materials. In the case of brittle materials Poisson ratio is less than 0.26. The calculated values of ν for Na_2SrSi and Na_2SrGe, which are 0.19, further support their brittle nature as determined by Pugh's ratio and Cauchy's pressure. Moreover, the Poisson's ratio also provides insights into the bonding nature of crystalline materials. Typically, materials with ionic bonds have a Poisson ratio around 0.25, while those with covalent bonds have a value around 0.1. Na_2SrX (Si and Ge) alloys appear to have covalent bonding properties based on the predicted value of ν. Young's modulus E measures the stiffness of a compound. We found that Young's modulus values for Na_2SrSi and Na_2SrGe are similar. The anisotropy factor A has an important role in engineering science. If A is equal to 1.0, the crystal is elastically isotropic, while any value other than one indicates anisotropy. The calculated value of A for the Na_2SrX (Si and Ge) alloys suggests that these compounds have a profound anisotropy.

The phonon dispersion curves of Na_2SrSi and Na_2SrGe compounds have been investigated and plotted in Fig. 3. Since these compounds have four atoms in their primitive cell, there are twelve phonon modes for each alloy. Three of them with lower frequency values are the acoustic modes and the rest are the optical modes. At their equilibrium structures, Na_2SrSi and Na_2SrGe crystals show no negative frequency. Thus, these compounds are dynamically stable.

3.3 Electronic properties

Figure 4 shows the band structure of Na_2SrX (Si and Ge) alloys calculated within GGA-mBJ approaches. As can be seen, the calculated electronic band structure with the optimized equilibrium lattice constant of the studied compounds shows similarities and exhibits a semiconductor behavior with an indirect band gap (L—X) of 0.652 eV and 0.629 eV for Na_2SrSi and Na_2SrGe, respectively. The band structure can be better understood using total

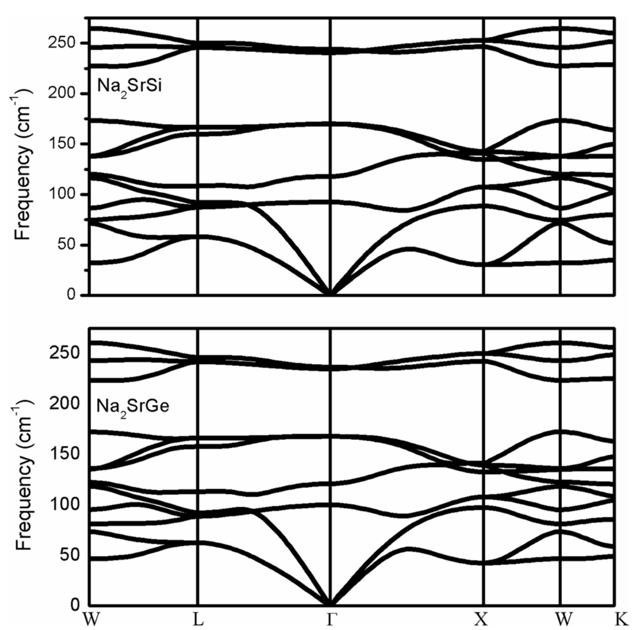

Fig. 3 Calculated phonon dispersion curves for Na_2SrSi and Na_2SrGe alloys

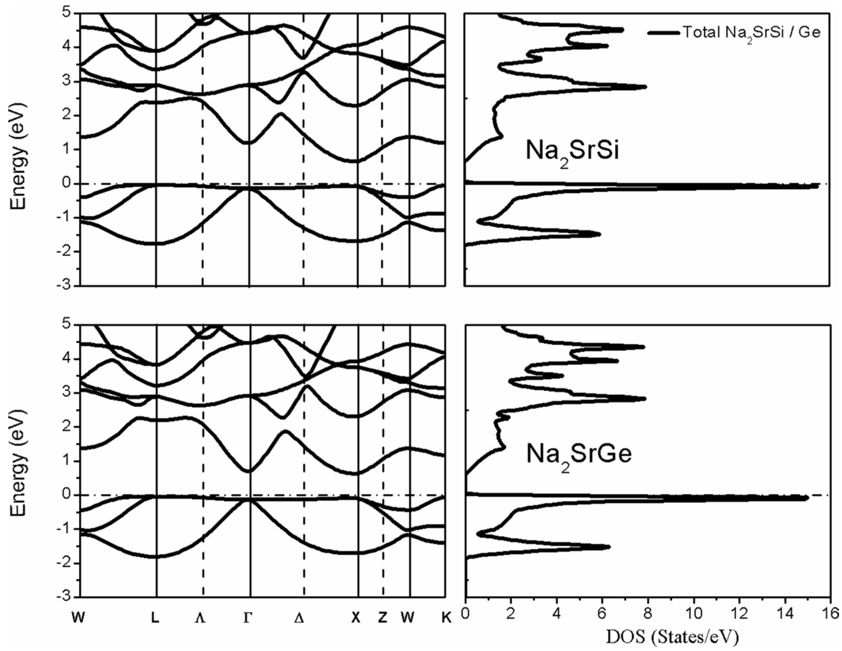

Fig. 4 Band structures and total densities of states (TDOS) of Na_2SrX (Si and Ge) alloys calculated within GGA-mBJ approaches

(TDOS) and partial (PDOS) densities of states. From Fig. 5, it is evident that the profiles of TDOS and PDOS of Na_2SrSi and Na_2SrGe compounds are similar. The Si-s band (Ge–s band) of Na_2SrSi (Na_2SrGe) is positioned at -5.5 eV (-6.36 eV). The region just below the Fermi energy level is related to Sr-d (d-t_{2g}) states and X-p states, but the major impact comes from Si-p (Ge-p). On the contrary, in the region above the Fermi energy level, the main contribution is dominated by Sr-d (d-t_{2g}) states, and the contributions of the X-p states are very low. The contribution of Na in the two regions is very small compared to Sr and Si (Ge) atoms.

Another significant quantity that affects the optoelectronic characteristics of materials and devices is the exciton binding energy (E_b) [59]. We computed the exciton binding energies of Na_2SrSi and Na_2SrGe using the Mott-Wannier model (WM) [60], which is applicable for inorganic semiconductors with a narrow band gap and a high dielectric constant. E_b is obtained from:

$$E_b = \frac{13.6\mu_r^*}{m_0\varepsilon_0^2} \tag{11}$$

where m_0 is the free electron mass, ε_0 is the static dielectric constant and μ_r^* is the reduced effective mass:

$$\frac{1}{\mu_r^*} = \frac{1}{m_e^*} + \frac{1}{m_h^*} \tag{12}$$

$m_{e/h}^*$ are the effective masses of the hole and electron. Thus, the effective mass can be computed using the relation:

$$\frac{1}{m^*} = \frac{1}{\hbar^2}\frac{\partial^2 E(k)}{\partial k^2} \tag{13}$$

The exciton binding energies are about 8.58 meV for Na_2SrSi and 6.91 meV for Na_2SrGe. The lower exciton binding energies obtained are comparable to those determined experimentally for GaAs (4.0 meV) [61] and GaSb (2.1 meV) [62], suggesting that both compounds are suitable for photovoltaic applications.

3.4 Optical properties

The interaction of light with a solid is described by its macroscopic optical properties. The optical properties (refractive index, reflectivity, energy loss spectra, optical conductivity, and optical absorption) are determined by the complex dielectric function $\varepsilon(\omega)$. Where, $\varepsilon(\omega)$ represents the linear response of matter to incident electromagnetic radiation of various frequencies. This function is given by:

$$\varepsilon(\omega) = \varepsilon_1(\omega) + i\varepsilon_2(\omega) \tag{14}$$

Here, $\varepsilon_1(\omega)$ and $\varepsilon_2(\omega)$ represent the real and imaginary parts of the dielectric function, respectively, and they are related by the Kramers–Kronig relations [63]. $\varepsilon_1(\omega)$ and $\varepsilon_2(\omega)$ of Na_2SrSi and Na_2SrGe under photon energies are shown in Fig. 6. We note that the spectra of the real and imaginary parts of the dielectric function of the two materials under study are almost identical and have the same peaks, with a slight difference in intensity. From the imaginary component, the threshold energy for optical transition

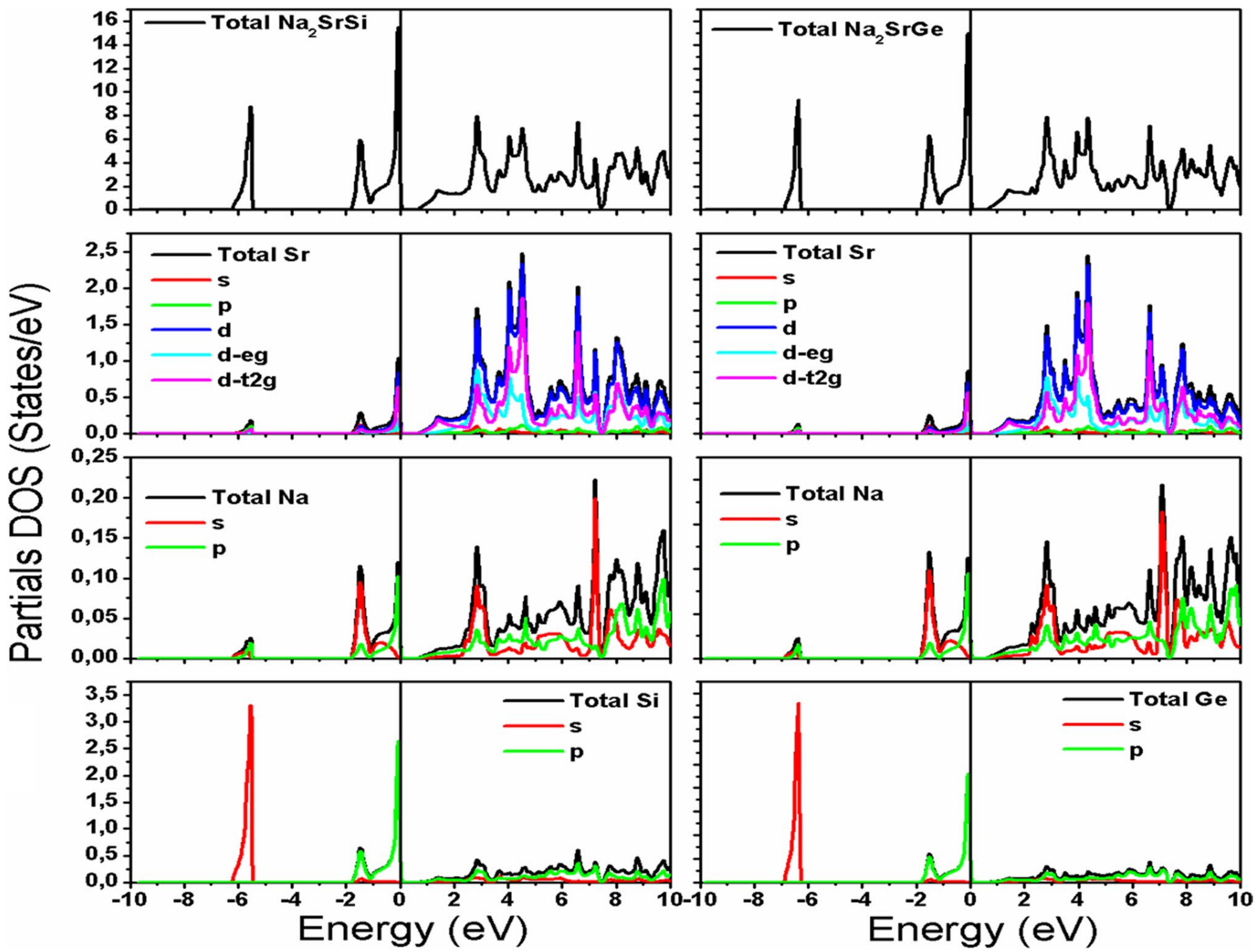

Fig. 5 Total (TDOS) and partial densities of states of states (PDOS) of Na_2SrX (Si and Ge) alloys calculated within GGA-mBJ approaches

Fig. 6 Calculated real ($\varepsilon_1(\omega)$) and imaginary ($\varepsilon_2(\omega)$) parts of the dielectric function, reflectivity and absorption for the Na_2SrX (Si and Ge) materials

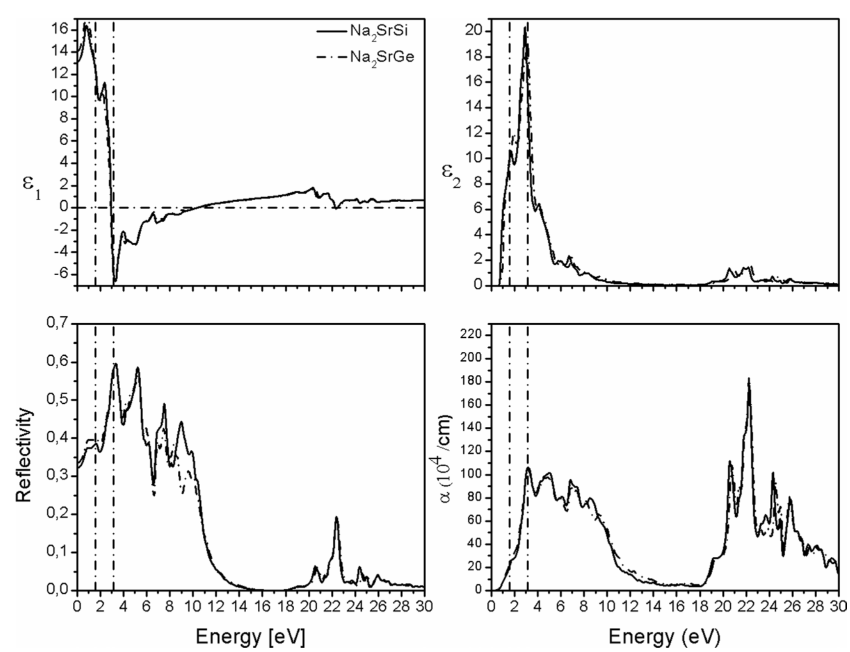

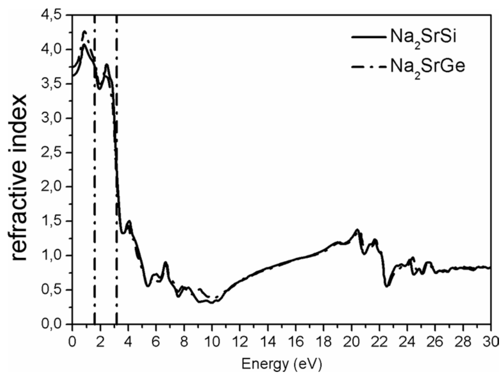

Fig. 7 Calculated refractive index for the Na_2SrX (Si and Ge) Heusler alloys

between the top of the valence band and the bottom of the conduction band, which represent the fundamental absorption edge, is found to be consistent with our calculated energy gap for these compounds. The electronic transitions from the p states of Si/Ge atoms to the unoccupied d states of the Sr atom are manifested as several peaks in the curve of $\varepsilon_2(\omega)$. Two main peaks of the $\varepsilon_2(\omega)$ spectrum of Na_2SrSi and Na_2SrGe occur approximately at the same position in the visible region, at 1.7 eV and 2.90 eV, which can be attributed to the same transitions. At zero frequency limits, we define the static dielectric constant $\varepsilon_1(0)$. The values of $\varepsilon_1(0)$ listed in Table 1 are inversely proportional to the band gap, which is consistent with the Penn model [64]. At low energies, where $\varepsilon_1(\omega)$ is positive, the electromagnetic wave propagates through the materials. The region where $\varepsilon_1(\omega) < 0$, is characterized by strong reflectivity and absorption. Figure 7 shows the refractive index dependence on energy of the incident radiation of Na_2SrX (Si and Ge) alloys. The variation of $n(\omega)$ with energy exhibits a similar trend to $\varepsilon_1(\omega)$, as both parameters are related to the amount of light that is absorbed by a material. For Na_2SrSi and Na_2SrGe, the maximum value of $n(\omega)$ is observed in the infrared domain of light spectrum at 0.8 eV (4.07) and 0.82 eV (4.26), respectively. The static values of refractive index $n(0)$ are about 3.62 for Na_2SrSi and 3.74 for Na_2SrGe. Our calculated static values of refractive index $n(0)$ and dielectric constant $\varepsilon_1(0)$ are consistent with those of some binary semiconductors such as GaAs and GaSb [61, 65, 66]. Hence, Na_2SrSi and Na_2SrGe have the potential for photovoltaic applications. From the spectrum of the energy dependence of the absorption (Fig. 4) for the two compounds, we notice that the absorption edges correspond very well to the band gaps. Na_2SrSi and Na_2SrGe are good absorbers in the ultraviolet region; there is no absorption peak in the IR and visible regions. The reflectivity follows a similar behavior to absorption; $R(\omega)$ shows also two bands; the first band is up to 13 eV and the second lies in the energy range (17.75–31 eV). Therefore, in the energy range (13–17.75 eV), the absorption is very low and the reflectivity is negligible, then these full Heulser compounds exhibit transparent properties. The obtained results suggest that these materials are beneficial for several applications, like optoelectronics.

4 Conclusion

In this paper, the FP-LAPW method based on density functional theory (DFT) was used to study the properties of Na_2SrX (X = Si and Ge) full-Heusler alloys. Structural, electronic, and optical properties at optimized equilibrium lattice constants are investigated. Calculations show that the Hg_2CuTi-type structure is energetically the most favorable for the two compounds. The electronic results showed that these compounds are semiconductors with an indirect band gap (L—X). The exciton binding energy of Na_2SrSi and Na_2SrGe alloys was found to be relatively small. The phonon dispersion calculations proved that in the ground state, Na_2SrGe and Na_2SrSi compounds are dynamically stable. Optical properties showed that Na_2SrSi and Na_2SrGe are promising materials for photovoltaic applications. The studied compounds are good absorbers in the ultraviolet region and exhibit a maximum reflectivity of about 60%. Therefore, we expect that the presented results can provide reliable data for further work and that the studied materials can be used in optoelectronic devices in the ultraviolet range.

Author Contributions All authors contributed to the study conception and design. The first draft of the manuscript was written by Charef Abbes and all authors commented on previous versions of the manuscript. All authors read and approved the final manuscript.

Funding The authors declare that no funds, grants, or other support were received during the preparation of this manuscript.

Declarations

Competing Interests The authors have no relevant financial or non-financial interests to disclose.

References

1. F. Heusler, Über magnetische Manganlegierungen. Verhandlungen Dtsch. Phys. Ges. **5**, 219 (1903)
2. C. Felser and A. Hirohata, Heusler Alloys: Properties, Growth, Applications, Springer Series in Materials Science 222, 2016 ISSN 2196–2812.
3. L. Bainsla and K.G. Suresh, Physics and Magnetism of Quaternary Heusler Alloys, Handbook of Magnetic Materials, Volume 25, Ekkes Brück (Eds.)- North Holland (2016). https://doi.org/10.1016/bs.hmm.2016.08.001
4. S. Benatmane, B. Bouhafs, investigation of new d0 half-metallic full-heusler alloys N2BaX (X = Rb, Cs, Ca and Sr) using

first-principle calculations. Comput. Condens. Matter. **16**, e00371 (2019). https://doi.org/10.1016/j.cocom.2019.e00371
5. I. Daniel, Blic, Geoffroy Hautier, David Waroquiers, Gian-Marco Rignanese, and Philippe Ghosez, Low-Dimensional Transport and Large Thermoelectric Power Factors in Bulk Semiconductors by Band Engineering of Highly Directional Electronic States. Phys. Rev. Lett. **114**, 136601 (2015). https://doi.org/10.1103/PhysRevLett.114.136601
6. X.R. Chen, M.M. Zhong, Y. Feng, Y. Zhou, H.K. Yuan, H. Chen, Structural, electronic, elastic, and thermodynamic properties of the spin-gapless semiconducting Mn2CoAl inverse Heusler alloy under pressure. Phys. Status Solidi B. **252**(12), 2830–2839 (2015). https://doi.org/10.1002/pssb.201552389
7. J.F. Herbst, M.S. Meyer, Structural, electronic, and hydriding properties of Li_2MgSi. J. All Com. **492**, 65–68 (2010). https://doi.org/10.1016/j.jallcom.2009.12.032
8. M. Matougui, B. Bouadjemi, M. Houari, A. Zitouni, T. Lantri, S. Haid, S. Bentata, B. Bouhafs, Z. Aziz, R. Khenata, Electronic structure, mechanical and thermoelectric properties of the full Heusler Ba_2AgZ (Z = Bi, Sb) alloys: insights from DFT study. Indian. J. Phys. **95**, 2675–2686 (2021). https://doi.org/10.1007/s12648-020-01943-9
9. S. Mesbah, M. Houari, F.Z. Boufadi, B. Bouadjemi, T. Lantri, S. Bentata, M. Ameri, Full Heusler alloys, with high absorption coefficient, insight into the optical properties of Li_2CaC and Li_2SrC. Solid. State. Commun. **328**, 114238 (2021). https://doi.org/10.1016/j.ssc.2021.114238
10. A.R. Mishra, S. Pal, First-principles calculations to investigate electronic structure and magnetic, mechanical and thermodynamic properties of d0 half-Heusler LiXN (X= Na, K, Rb) alloys. Solid State Sci. **118**, 106633 (2021). https://doi.org/10.1016/j.solidstatesciences.2021.106633
11. M. Jubair, A.M.M. Tanveer Karim, M. Nuruzzaman, M. Roknuzzaman, M.A.K. Zilani, Pressure dependent structural, elastic and mechanical properties with ground state electronic and optical properties of half-metallic Heusler compounds Cr_2YAl (Y = Mn, Co): first-principles study. J. Heliyon. **7**, e08585 (2021). https://doi.org/10.1016/j.heliyon.2021.e08585
12. T.M. Bhat, M. Nabi, D.C. Gupta, Structural, elastic, thermodynamic and thermoelectric properties of Fe_2TiSn Heusler alloy: high pressure study. Results in Physics. **12**, 15–20 (2019). https://doi.org/10.1016/j.rinp.2018.11.041
13. A. Dehghan, S. Davatolhagh, First principles study of d^0-d half-Heusler alloys containing group-IV, -V, and -VI sp atoms as prospective half-metals for real spintronic applications. Mat. Chem. Phys. **273**, 125064 (2021). https://doi.org/10.1016/j.matchemphys.2021.125064
14. D. Shrivastava, S.P. Sanyal, Electronic, phonon and superconducting properties of LaPtBi half-Heusler compound. Solid State Commun. **273**, 1–4 (2018). https://doi.org/10.1016/j.ssc.2018.01.018
15. S. Singh, D.C. Gupta, Magneto-electronic, thermoelectric, thermodynamic and optical properties of rare earth YCoTiX (X = Al, Ga, Si, Ge) alloys. J. Alloy. Compd. **806**, 1292–1308 (2019). https://doi.org/10.1016/j.jallcom.2019.07.303
16. S. Tabassam, A.H. Reshak, G. Murtaza, S. Muhammad, A. Laref, M. Yousaf, A.M. AlBakri, J. Bila, Co_2YZ (Y = Cr, Nb, Ta, V and Z = Al, Ga) Heusler alloys under the effect of pressure and strain. J. Mol. Graphics Modelling. **104**, 107841 (2021). https://doi.org/10.1016/j.jmgm.2021.107841
17. T. Graf, C. Felser, S.S. Parkin, Simple rules for the understanding of Heusler compounds. Prog. Solid. State. Chem. **39**, 1–50 (2011). https://doi.org/10.1016/j.progsolidstchem.2011.02.001
18. I. Galanakis, P.H. Dederichs, N. Papanikolaou, Slater-Pauling behavior and origin of the half-metallicity of the full-Heusler alloys. Phys. Rev. B. **66**, 174429 (2002). https://doi.org/10.1103/physrevb.66.174429
19 J.Y. Jong, J. Zhu, Su.-Il. Pak, G.H. Sim, Theoretical Investigation of Mechanical, Electronic, and Thermal Properties of Fe_2TiSi and Fe_2TiSn Under Pressure. J. Electron. Mater. **45**, 5104–5111 (2016). https://doi.org/10.1007/s11664-016-4722-z
20. J. Jalilian, G. Rezaei, B. Vaseghi, F. Kanjouri, S. Fakhri, A. Ramazani, Tunable indirect to direct band gap transition of Fe_2TaX (X=Al and Ga) Heusler alloy under hydrostatic pressure effect. Comput. Mater. Sci. **203**, 111049 (2022). https://doi.org/10.1016/j.commatsci.2021.111049
21. high pressure study, M. Bhat, T. Nabi, M., Gupta, D.C., Structural, elastic, thermodynamic and thermoelectric properties of Fe_2TiSn Heusler alloy. Results in Physics. **12**, 15–20 (2019). https://doi.org/10.1016/j.rinp.2018.11.041
22. S. Krishnaveni, M. Sundareswari, Band gap engineering in ruthenium-based Heusler alloys for thermoelectric applications. Int. J. Energy. Res. **42**, 764–775 (2018). https://doi.org/10.1002/er.3864
23. A. Guezmir, H. Rached, A. Bentouaf, M. Caid, N. Benkhettou, D. Rached, M. Sidoumou, Theoretical insight of stabilities and optoelectronic features of Ru-based Heusler alloys: Ab-initio calculations. Comput. Cond. Matter. **28**, e00573 (2021). https://doi.org/10.1016/j.cocom.2021.e00573
24 E. Enamullah, P.R. Cha, The n- and p-type thermoelectric response of a semiconducting Co-based quaternary Heusler alloy: a density functional approach. J. Mater. Chem. C. **7**, 7664–7671 (2019). https://doi.org/10.1039/C9TC00570F
25. S.A. Khandy, I. Islam, D.C. Gupta, R. Khenata, A. Laref, Lattice dynamics, mechanical stability and electronic structure of Fe-based Heusler semiconductors. Sci. Rep. **9**, 1475 (2019). https://doi.org/10.1038/s41598-018-37740-y
26. S. Sharma, S.K. Pandey, Investigation of the electronic and thermoelectric properties of Fe_2ScX (X = P, As and Sb) full Heusler alloys by using first principles calculation. J. Phys. D: Appl. Phys. **47**, 445303 (2014). https://doi.org/10.1088/0022-3727/47/44/445303
27. J. He, S.S. Naghavi, V.I. Hegde et al., Designing and discovering a new family of semiconducting quaternary heusler compounds based on the 18-electron rule. Chem Mater. **30**(15), 4978–4985 (2018). https://doi.org/10.1021/acs.chemmater.8b01096
28. J. Singh, K. Kaur, S.A. Khandy, S. Dhiman, M. Goyal, S.S. Verma, Structural, electronic, mechanical, and thermoelectric properties of LiTiCoX (X = Si, Ge) compounds. Int. J. Energy. Res. **45**(11), 16891–16900 (2021). https://doi.org/10.1002/er.6851
29. J. Singh, K. Kaur, S.A. Khandy, M. Goyal, S. Dhiman, S.S. Verma, Structural, electronic, vibrational, thermoelectric and mechanical properties of Li based quaternary Heusler compound LiTiCoSn: A DFT approach. Mater. Today: Proceedings. **57**, 211–216 (2022). https://doi.org/10.1016/j.matpr.2022.02.358
30. J. Singh, K. Kaur, M.A. Bhat, U.B. Sharopov, S. Dhiman, M. Goyal, S.S. Verma, S.A. Khandy, First-principles calculations on the electronic structure and thermoelectric properties of quaternary Heusler compounds: LiScPtSi and LiScPdGe. Mater. Today Communications. **32**, 103961 (2022). https://doi.org/10.1016/j.mtcomm.2022.103961
31. T. Kaur, J. Singh, M. Goyal, K. Kaur, S.A. Khandy, M.A. Bhat, U.B. Sharopov, S. Dhiman, A.F. Wani, B. Rani, M.M. Sinha, S.S. Verma, First principles calculation to investigate Li based quaternary Heusler compounds LiHfCoX (X= Ge, Sn) for thermoelectric applications. Phys. Scr. **97**, 105706 (2022). https://doi.org/10.1088/1402-4896/ac8c70
32. M. Mushtaq, M.A. Sattar, S.A. Dar, Phonon phase stability, structural, mechanical, electronic, and thermoelectric properties of two new semiconducting quaternary Heusler alloys CoCuZrZ (Z = Ge and Sn). Int. J. Energy. Res. **44**, 5936–5946 (2020). https://doi.org/10.1002/er.5373

33. J. He, M. Amsler, Y. Xia, S.S. Naghavi, V.I. Hegde, S. Hao, S. Goedecker, V. Ozoliņš, C. Wolverton, Ultralow Thermal Conductivity in Full-Heusler Semiconductors. Phys. Rev. Lett. **117**, 046602 (2016). https://doi.org/10.1103/PhysRevLett.117.046602
34. S. Mesbah, M. Houari, F.Z. Boufadi, B. Bouadjemi, T. Lantri, S. Bentata, M. Ameri, Full Heusler alloys, with high absorption coefficient, insight into the optical properties of Li_2CaC and Li_2SrC. Solid. State. Commun. **328**, 114238 (2021). https://doi.org/10.1016/j.ssc.2021.114238
35. J.F. Herbst, M.S. Meyer, Structural, electronic, and hydriding properties of Li_2MgSi. J Alloys. Compd. **492**, 65–68 (2010). https://doi.org/10.1016/j.jallcom.2009.12.032
36. P. Hohenberg, W. Kohn, Inhomogeneous Electron Gas. Phys. Rev. 136, B864 (1964). https://link.aps.org/doi/10.1103/PhysRev.136.B864
37. W. Kohn, L.J. Sham, Self-Consistent Equations Including Exchange and Correlation Effects.Phys. Rev. 140, A1133 (1965). https://link.aps.org/doi/10.1103/PhysRev.140.A1133
38. P. Blaha, K. Schwarz, P. Sorantin, Full-potential, linearized augmented plane wave programs for crystalline systems. Comput. Phys. Commun. **59**, 399–415 (1990). https://doi.org/10.1016/0010-4655(90)90187-6
39. P. Blaha, K. Schwarz, G.K. Madsen, D. Kvasnicka, J. Luitz, R. Laskowsk, F. Tran, L. Marks, L. Marks, *WIEN2k: An Augmented Plane Wave plus Local Orbitals Program for Calculating Crystal Properties* (Universitat, Techn, 2019)
40. J.P. Perdew, K. Burke, M. Ernzerhof, Generalized Gradient Approximation Made Simple. Phys. Rev. Lett. 77, 3865-3868 (1996). https://link.aps.org/doi/10.1103/PhysRevLett.77.3865
41. F. Tran, P. Blaha, Accurate Band Gaps of Semiconductors and Insulators with a Semilocal Exchange-Correlation Potential. Phys. Rev. Lett. 102, 226401 (2009). https://link.aps.org/doi/10.1103/PhysRevLett.102.226401
42. H.J. Monkhorst, J.D. Pack, Special points for Brillouin-zone integrations. Phys. Rev. B. 13, 5188–5192 (1976). https://link.aps.org/doi/ https://doi.org/10.1103/PhysRevB.13.5188
43. S. Baroni, P. Giannozzi, and A. Testa, Green's-function approach to linear response in solids. Phys. Rev. Lett. 58, 1861–1864 (1987). https://doi.org/10.1103/PhysRevLett.58.1861
44. P. Giannozzi, S. de Gironcoli, P. Pavone, and S. Baroni, Ab initio calculation of phonon dispersions in semiconductors. Phys. Rev. B. 43, 7231–7242 (1991). https://link.aps.org/doi/ https://doi.org/10.1103/PhysRevB.43.7231
45. X. Gonze, Adiabatic density-functional perturbation theory. Phys. Rev. A. 52, 1096–1114 (1995). https://link.aps.org/doi/10.1103/PhysRevA.52.1096
46. X. Gonze, Erratum: Adiabatic density-functional perturbation theory. Phys. Rev. A. **54**, 4591 (1996). https://doi.org/10.1103/physreva.54.4591
47. S. Baroni, S. de Gironcoli, A. Dal Corso, P. Giannozzi, Phonons and Related Crystal Properties from Density-Functional Perturbation Theory. Rev. Mod. Phys. **73**, 515–562 (2001). https://doi.org/10.1103/RevModPhys.73.515
48. P. Giannozzi, S. Baroni, N. Bonini, M. Calandra, R. Car, C. Cavazzoni, D. Ceresoli, G.L. Chiarotti, M. Cococcioni, I. Dabo, QUANTUM ESPRESSO: a modular and open-source software project for quantum simulations of materials. J. Phys. Condens. Matter. **21**(39), 395502 (2009). https://doi.org/10.1088/0953-8984/21/39/395502
49 P. Giannozzi, O. Andreussi, T. Brumme, O. Bunau, M.B. Nardelli, M. Calandra, R. Car, C. Cavazzoni, D. Ceresoli, M. Cococcioni, Advanced capabilities for materials modelling with Quantum ESPRESSO. J. Phys. Condens. Matter. **29**(46), 465901 (2017). https://doi.org/10.1088/1361-648X/aa8f79
50. K.F. Garrity, J.W. Bennett, K.M. Rabe, D. Vanderbilt, Pseudopotentials for high-throughput DFT calculations. Comput. Mater. Sci. **81**, 446–452 (2014). https://doi.org/10.48550/arXiv.1305.5973
51. F.D. Murnaghan, The Compressibility of Media under Extreme Pressures. Proc. Natl. Acad. Sci. U.S.A. **30**, 244–247 (1944). https://doi.org/10.1073/pnas.30.9.244
52. S. Belbachir, C. Abbes, M.N. Belkaid, A.H. Belbachir, First-Principle Study of Structural, Elastic, Electronic and Magnetic Properties of the Quaternary Heusler CoZrFe. J. Supercond. Nov. Magn **33**, 2899–2905 (2020). https://doi.org/10.1007/s10948-020-05598-9
53. C. Abbes, S. Belbachir, H. Abbassa, S. Meskine, A. Boukra, A. Boukortt, Robust half-metallicity in CoZrMnZ (Z= P, As and Sb) quaternary Heusler alloys. Phil. Mag. **101**(7), 892–904 (2020). https://doi.org/10.1080/14786435.2021.1872809
54. Y. Pan, X. Chen, X. Zhang, Tailoring the hydrogenated mechanism of Pt_3Al from first-principles investigation. Vacuum **212**, 112033 (2023). https://doi.org/10.1016/j.vacuum.2023.112033
55. M. Born, K. Huang, *Dynamical Theory and Experiment I* (Springer-Verlag, Berlin, 1982)
56. W. Voigt, *Lehrbuch der Kristallphysik* (Taubner, Leipzig, 1928)
57. A. Reuss. Math. Mech. 9, 49–58 (1929) 49. https://doi.org/10.1002/zamm.19290090104
58. R. Hill, The elastic behaviour of a crystalline aggregate. Proc. Phys. Soc. **65**, 349–354 (1952). https://doi.org/10.1088/0370-1298/65/5/307
59. L. Xu, G. Liu, H. Xiang, R. Wang, Q. Shan, S. Yuan, B. Cai, Z. Li, W. Li, S. Zhang, H. Zeng, Charge-carrier dynamics and regulation strategies in perovskite light-emitting diodes: From materials to devices. App. Phy. Rev **9**, 021308 (2022). https://doi.org/10.1063/5.0080087
60. N. W. Ashcroft and N. D. Mermin, Solid State Physics (Saunders College, Fort Worth, 1976). ISBN 0–03–083993–9
61. J.S. Blakemore, Semiconducting and other major properties of gallium arsenide. J. Appl. Phys. **53**, R123–R181 (1982). https://doi.org/10.1063/1.331665
62 P.P. Paskov, Optical absorption and refraction spectra in highly excited GaSb. IEEE J. Quantum Electron. **30**, 2771–2777 (1994). https://doi.org/10.1109/3.362734
63. Safa Kasap, Peter Capper, Springer Handbook of Electronic and Photonic Materials, 2006 Edition, e-ISBN: 0–387–29185–7
64. D. R. Penn, Wave-number-dependent dielectric functions of semiconductors. Phys. Rev.128, 2093–2097 (1962). https://link.aps.org/doi/10.1103/PhysRev.128.2093
65. S. Kacimi, H. Mehnane, A. Zaoui, I-II–V and I–III–IV half-Heusler compounds for optoelectronic applications: Comparative ab initio study. J Alloys Compd. **587**, 451–458 (2014). https://doi.org/10.1016/j.jallcom.2013.10.046
66. J.B. Theeten, D.E. Aspnes, R.P.H. Chang, A new resonant ellipsometric technique for characterizing the interface between GaAs and its plasma-grown oxide. J. Appl. Phys. **49**, 6097–6102 (1978). https://doi.org/10.1063/1.324529

Springer Nature or its licensor (e.g. a society or other partner) holds exclusive rights to this article under a publishing agreement with the author(s) or other rightsholder(s); author self-archiving of the accepted manuscript version of this article is solely governed by the terms of such publishing agreement and applicable law.